JCTC Journal of Chemical Theory and Computation

Conformational Analysis of Arabinofuranosides: Prediction of $^3J_{H,H}$ Using MD Simulations with DFT-Derived Spin−Spin Coupling Profiles

Hashem A. Taha,[†] Norberto Castillo,[†] Devin N. Sears,[†] Roderick E. Wasylishen,[†] Todd L. Lowary,*[,†] and Pierre-Nicholas Roy*[,‡]

Department of Chemistry and Alberta Ingenuity Centre for Carbohydrate Science, Gunning-Lemieux Chemistry Centre, University of Alberta, Edmonton, AB, Canada T6G 2G2, and Department of Chemistry, University of Waterloo, Waterloo, ON, Canada N2L 3G1

Received September 9, 2009

Abstract: A molecular dynamics (MD) investigation on a series of oligo-α-arabinofuranosides (**1**−**8**) using the AMBER force field and the GLYCAM carbohydrate parameter set is reported. The validation of the method was carried out by direct comparison of experimental vicinal proton−proton coupling constants ($^3J_{H,H}$) with those obtained by using an empirically determined Karplus equation and density functional theory (DFT)-derived relationships specifically tailored for α-arabinofuranosyl systems. A simple code was developed to implement the determination of $^3J_{H,H}$ by applying these relationships to the probability distributions of rotamers and ring conformations displayed by the simulations. The empirical Karplus relationship and the DFT-derived equations yielded, in most cases, the same trend as experiment for intra-ring $^3J_{H,H}$ values. This direct comparison circumvents additional sources of errors that may arise from the assumptions introduced by the deconvolution procedures often used to calculate population of rotamers and ring conformations from experimental $^3J_{H,H}$.

Introduction

Molecular dynamics (MD) simulations of glycoconjugates are an active area of research due to the role of carbohydrate-containing molecules in several life processes,[1−4] and it is now appreciated that the conformational preferences of these molecules are critical determinants of their biological activity.[5,6] The conformational analysis of complex carbohydrates is often too complex and challenging to be addressed completely by experimental methods and thus such investigations rely heavily on the tandem use of computational and experimental approaches (largely NMR spectroscopy and X-ray crystallography).[5,6] To complement these techniques, significant efforts have therefore been devoted to studying the conformational equilibrium of carbohydrates computationally.

Various accounts have described the development of methodologies for deriving force field parameters, including atomic charges, to simulate biomolecules,[7−12] and there are extensive reports describing molecular dynamics simulations on oligosaccharides containing pyranoside (six-membered) rings.[13−17] Software programs for the structural prediction of sugars have also been developed to investigate possible conformations not visited by nonergodic simulations.[18−20] Far fewer investigations of oligosaccharides containing one or more furanose (five-membered) rings have been reported.[21−27]

Our group has a long-standing interest in the furanoside-containing polysaccharides that are found in the cell wall structure of mycobacteria, including the pathogenic species *Mycobacterium tuberculosis* and *Mycobacterium leprae,* which cause tuberculosis and leprosy, respectively.[28] These glycoconjugates play a critical role in mycobacterial survival and pathogenicity. Conformational investigations of these molecules are of interest as the information gleaned will be of help in developing inhibitors of enzymes that process

* To whom correspondence should be addressed. E-mail: pnroy@uwaterloo.ca, todd.lowary@ualberta.ca.

[†] University of Alberta.

[‡] University of Waterloo.

10.1021/ct900477x
Published on Web 12/02/2009

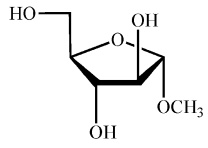

1

$$\tan P = \frac{(\phi_2 + \phi_4) - (\phi_1 + \phi_3)}{3.077\phi_0}$$

$$\phi_m = \frac{\phi_0}{\cos P}$$

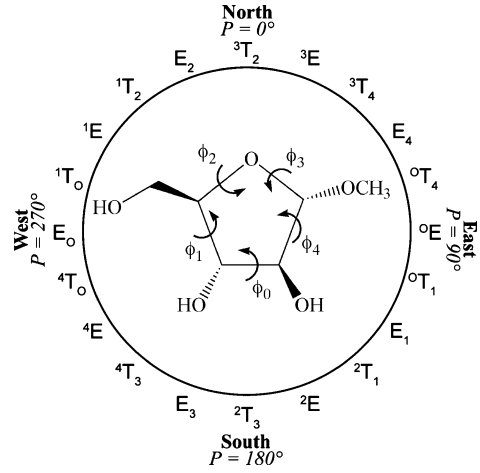

Figure 1. Pseudorotational itinerary for methyl α-D-arabinofuranoside, **1**.

furanose sugars.[29] However, conformational studies of oligofuranosides are more complex than comparable investigations on oligopyranosides, due to the inherent flexibility of five-membered rings.[21−26]

Furanoside rings can adopt a number of twist (T) and envelope (E) conformations, which can be depicted using the pseudorotational itinerary (Figure 1). Each conformer can be described by two coordinates: the Altona−Sundaralingam (AS) phase angle of pseudorotation (P), which represents the atoms that are displaced from the plane, and the AS puckering amplitude (ϕ_m), a measure of the maximum displacement from the planar ring form.[30] Given five endocyclic torsion angles of a given conformer, P and ϕ_m can be calculated through the use of the equations shown in Figure 1.[30] The interconversion barrier between these conformers is relatively low (<5 kcal/mol),[31] and this flexibility renders the theoretical description of furanosides challenging, as one must consider both the torsion angles of the ring (Figure 1) as well as any exocyclic dihedral angles.

Determination of the solution conformation of carbohydrates is most frequently performed using NMR spectroscopy,[32−34] and great effort has been devoted to the study of molecular conformations by analysis of both homo- and heteronuclear NMR coupling constants and their orientational dependence.[32−44] Experimental coupling constants, $^3J_{H,H}$, are measured as an average over the entire conformational space of the molecule and this average can be expressed by eq 1[45]

$$\langle J \rangle = \int_0^{360} J(\phi)\, \rho(\phi)\, \mathrm{d}\phi \qquad (1)$$

where $J(\phi)$ is an extended Karplus equation that correlates the vicinal nuclear spin−spin coupling constants to the dihedral angle between the coupled spins and $\rho(\phi)$ is the probability distribution of dihedral angles about a particular bond.

The simplest method for assessing conformation about acyclic fragments is the "discrete model".[45] In this approach, it is assumed that a set of equilibrating rotamers of discrete dihedral angles (usually three staggered rotamers) adequately describes the conformational preferences about that bond. As an example, for the C4−C5 bond in methyl α-D-arabinofuranoside (**1**), three staggered rotamers about this bond, gt, tg, and gg, can be defined (Figure 2) and are generally used in calculations of this type.

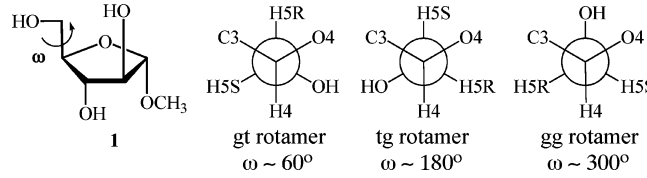

Figure 2. Definitions of the three staggered rotamers about the C4−C5 bond in **1**. The angle ω is defined as the O5−C5−C4−O4 torsion angle.

This approach is formally expressed by eq 2, where X_i (i = 1, 2, 3) are the unknown populations of the discrete rotamers, ϕ_i is the H4−C4−C5−H5*R* or H4−C4−C5−H5*S* dihedral angle in each of the three rotamers, and $\langle J \rangle$ is the measured average coupling constant.

$$\langle J \rangle = \sum_{i=1}^{3} X_i J(\phi_i) \quad \text{with} \quad \sum_{i=1}^{3} X_i = 1 \qquad (2)$$

This assumption leads to potential errors in the analysis, because it does not consider deviations from the staggered conformations and does not account for contributions from dihedral angles with low probability. In addition, for some systems more than three conformers may exist.

The search for alternatives to address the limitations arising from assumptions of the discrete model and thus to better define $\rho(\phi)$ gave rise to the generation of continuous models. The continuous probability distribution (CUPID)[45] is among the most popular continuous models used.[35] This method is based on the fact that the probability distribution of rotamers, $\rho(\phi)$, must be a periodic function of ϕ and therefore can be expressed as a Fourier series where the coefficients of the expansion are the parameters to be determined from eq 1. For practical reasons, the Fourier series must be truncated, and this constitutes the main limitation of the method. Aside from its use in determining rotamer populations about single bonds, CUPID has been adapted for use in the conformational analysis of five-membered ring systems (CUPID-5), incorporating the general principles of pseudorotation.[46] The use of CUPID-5 yielded generally more accurate fits to the experimental NMR coupling constants, compared to discrete

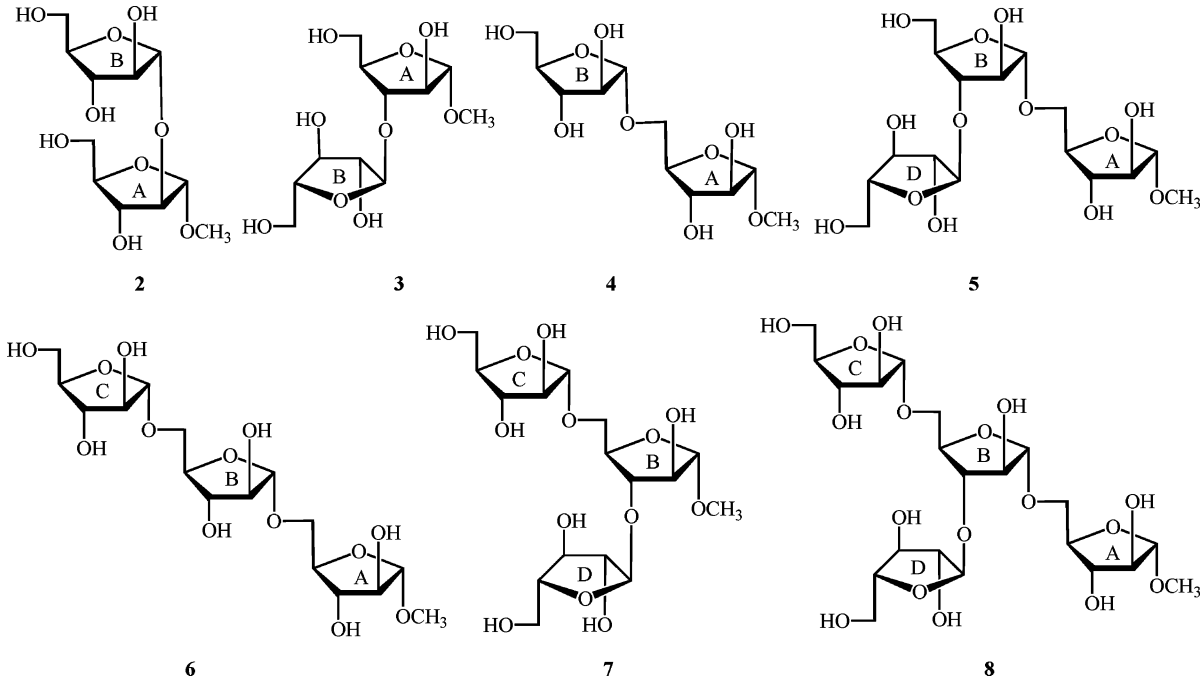

Figure 3. Oligoarabinofuranosides studied; rings have been lettered to facilitate comparison with **1**.

model approaches, e.g., PSEUROT analysis,[47] which assumes a two-state equilibrium for the five-membered ring.

The solution conformation of carbohydrates depends heavily on the interaction between the hydroxyl groups and solvent molecules.[48,49] Such interactions exhibit a strong electrostatic character (i.e., H-bonding) and thus requires a reliable set of atomic charges to properly model carbohydrates and to obtain acceptable simulation results compared to experiment.[50,51] Previously, we reported a procedure to obtain a set of atomic charges representative of the conformational equilibrium of **1**,[52] which has also been successfully applied to methyl β-D-arabinofuranoside.[53] This procedure reduced conformer-dependent charge variability, leading to better agreement between the C4−C5 bond rotamer distributions obtained from the MD simulations with those determined from NMR spectroscopic data.[54,55] In addition, these studies allowed us to gain insight into the ring conformation of **1** and its β anomer. However, here the agreement in the value of the pseudorotational phase angle, *P*, with experiment was less good. In particular for **1**, the MD simulations predicted a broad distribution of conformers centered around a single region of conformational space, whereas PSEUROT analysis of available $^3J_{H,H}$ data predicted an approximately 1:1 ratio of two conformers.

We describe here the use of probability distributions obtained from molecular dynamics simulations of **1** as the basis for calculating Boltzmann-averaged $^3J_{H,H}$ values using eq 1, which were then compared to those obtained experimentally. In one approach, we used an available generalized Karplus equation[56] (eq 3) for correlating each ring and exocyclic dihedral angle in all MD-derived conformers of **1** with $^3J_{H,H}$ values.

$$^3J_{HH} = 14.63\cos^2\phi - 0.78\cos\phi + 0.60 + \sum_i \lambda_i\{0.34 - 2.31\cos^2[\xi_i\phi + 18.4|\lambda_i|]\} \quad (3)$$

In this equation, ϕ is the dihedral angle between the coupled protons, λ_i is the difference in electronegativities between a non-hydrogen substituent *i* and hydrogen, and ξ_i is equal to ± 1 depending on the relative orientation of substituents along the coupling path. A limitation of this approach is that the equation used for deriving these "Karplus relationships" was generated empirically by analyzing various substituted ethane fragments possessing a range of substituents with varying electronegativity. Thus, although this equation is generalizable, we questioned if better correlation of conformation and $^3J_{H,H}$ for **1** and larger oligomers could be obtained by using relationships more tailored to the α-arabinofuranose ring system. Hence, using density functional theory (DFT) calculations, we derived spin−spin coupling relationships for each ethanic fragment in **1**, which were then used in the calculation of $^3J_{H,H}$ values. Better agreement with experiment was indeed found using the DFT-derived equations. With this method in hand, we carried out MD simulations on a set of oligofuranosides (**2**−**8**, Figure 3) to determine the robustness of the method in these larger molecules.

Methods

Nomenclature. For clarity we will refer to the C4−C5 rotamers of each unit in the oligofuranosides as the rotamers of the corresponding ring, although they are not completely contained in these rings.

DFT $^3J_{H,H}$ Coupling Profiles. The accurate measurement of spin−spin coupling constants has aided in the structure determination of various molecules ranging from small organic molecules to large proteins.[57−63] The difficulty in calculating the spin−spin coupling tensor, which describes the interactions of nuclei through their interactions with the electrons of the molecule, arises from (1) the several mechanisms[64,65] that all contribute to the spin−spin coupling

tensor and therefore cannot be neglected a priori and (2) the involvement of not only singlet excitations (similar to those found in the expressions for shielding) but triplet excitations, which are nearly impossible to accurately calculate in the Hartree−Fock approximation. Therefore, a theoretical framework in which electron correlation is taken into consideration must be used for this purpose. For a detailed discussion of the calculation of spin−spin coupling constants and the implementation in quantum mechanical software packages, the reader is referred to reviews by Vaara et al.,[65] Autschbach and Le Guennic,[64] and Helgaker et al.[66,67,69]

DFT calculations of the spin−spin coupling constants were performed using the Gaussian 03 program[68] at the B3LYP/cc-pVTZ level of theory.[69,70] This level of theory was chosen on the basis of the results of $^3J_{H,H}$ calculations for ethane using several different functionals and basis sets (see Supporting Information). For these calculations, 10 envelope conformers of **1** were constructed; three C4−C5 rotamers and three C5−O5 rotamers were generated for each envelope, giving a total of 90 conformations. The geometries of all 90 conformations were then optimized at the B3LYP/6-31G* level of theory. A single endocyclic torsion angle (representing the four-atom plane of each envelope conformer) was fixed at 0° to maintain the envelope structure. For example, the E_O conformer was generated by fixing C1, C2, C3, and C4 in the plane. All other geometric parameters were allowed to vary during the geometry optimizations. In all cases, the preoptimized geometries were built to minimize intramolecular hydrogen bonds, i.e., the O−H bond of the C-3 hydroxyl group is oriented anti to C-4. This structural motif was maintained through all optimizations for the entire set of furanosides. For the spin−spin coupling calculations, all four contributions to the $^3J_{H,H}$ were computed, including Fermi contact (FC), spin dipolar (SD), paramagnetic spin−orbital (PSO), and diamagnetic spin−orbital (DSO). The resulting *J* data were extracted for all conformations (see Supporting Information for complete coupling constant data).

For a picture of the structural dependencies of $^3J_{H,H}$ on their respective H,H torsion angles, the Marquardt−Levenberg nonlinear least-squares algorithm[71] was used to fit the acquired coupling constants to a truncated Fourier series in the H,H dihedral angle (ϕ) (eq 4)[72]

$$^3J_{HH} = a + b\cos(\phi) + c\cos(2\phi) \quad (4)$$

The coefficients *a*, *b*, and *c* can be determined from the fitting of the DFT data, and five equations can be obtained corresponding to the five three-bond H,H coupling pathways in the molecule (H1−C1−C2−H2, H2−C2−C3−H3, H3−C3−C4−H4, H4−C4−C5−H5*R*, H4−C4−C5−H5*S*).

Molecular Dynamics (MD) Simulations. All MD simulations were performed with the SANDER module of the AMBER 9.0 suite of programs[73] using the parm99 force field together with the GLYCAM (version 04f) parameters for carbohydrates.[74,75] The topology of the oligofuranosides was built by using the additivity principle[76,77] to the set of atomic charges obtained for monosaccharide **1**, which were determined, as previously reported,[52] to account for the flexibility of the ring. The starting geometries were also constructed from multiple units of **1** using the Leap module in AMBER. The simulations were carried out in water and under NPT conditions coupled to an external temperature bath[78] at 300 K and to a pressure bath at 1 atm to be consistent with the NMR data available. Each oligofuranoside was put in a theoretical box of approximate dimensions of 30 Å × 30 Å × 30 Å filled with TIP3P[79] water. We used periodic boundary conditions and the SHAKE[80] algorithm to fix all hydrogen-containing bonds to their equilibrium value. A dielectric constant of unity was used and a cutoff of 8 Å was set for nonbonded (short- and long-range) interactions. The particle mesh Ewald algorithm was used for treatment of long-range electrostatics.[81,82]

The simulations were started by first minimizing the energy of the water molecules with the geometry of the sugar molecules constrained. This was followed by a total energy minimization. Fifty cycles of steepest decent energy minimization followed by 950 cycles of conjugate gradient were applied to these first two steps. An annealing run of 100 ps was further applied followed by a short equilibration MD run of 150 ps. After this short MD run, production dynamics were performed up to 240 ns keeping the same temperature and pressure of 300 K and 1 atm, respectively.

In our earlier work,[52,53] simulation times of over 200 ns were required to obtain accurate rotamer distributions. Moreover, the convergence of the gt:tg:gg populations as a function of simulation time was used to establish this >200 ns criterion used in the present research. Shorter simulations will result in errors of several units of percentage on the rotamer populations. New methodologies will be required in order to analyze larger oligomers to avoid prohibitive simulation times.

Calculation of $^3J_{H,H}$ Values from Conformational Ensembles Obtained from MD Simulations. For an accurate comparison of the DFT/MD-derived $^3J_{H,H}$ values to experiment, ensemble averaging must be carried out. This was done by calculating $^3J_{H,H}$ values for each relevant bond in compounds **1**−**8** using the DFT-determined equations and the generalized Karplus equation previously developed by Altona and co-workers (eq 3).[56] These $^3J_{H,H}$ values were then ensemble-averaged using eq 1.

Results and Discussion

Spin−Spin Coupling Profiles. The spin−spin coupling constant data were plotted as a function of the respective H,H torsion angles and fitted to eq 4 (Figures 4 and 5). Each curve resulted in an equation, which correlates the $^3J_{H,H}$ magnitude with each dihedral angle (eqs 5−9). The coupling profiles for the ring protons (Figure 4 and eqs 5−7) show reasonably well fitted curves, although it is apparent that the curves are not well parametrized at torsion angles near 0° (±90°). It should be appreciated, however, that these equations are well-defined *only* over the area of rotational space that is possible given the constraints of this ring system. In addition, in all of the dihedral angle distributions generated from the MD conformer ensemble, no conformers that adopt these configurations are visited (see Supporting Information). For angles that cannot be obtained while the ring structure

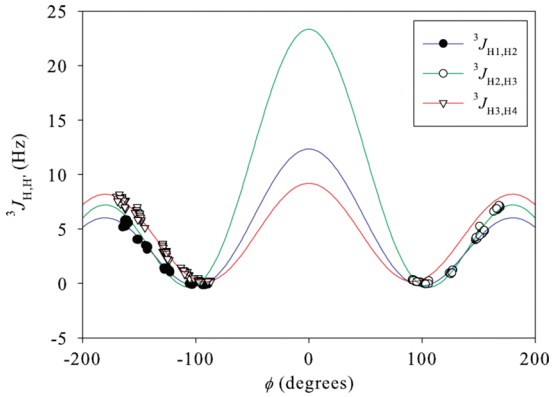

Figure 4. $^3J_{H,H}$ coupling profiles for the ring protons of methyl α-D-arabinofuranoside. All fits resulted in an R^2 value of 0.99.

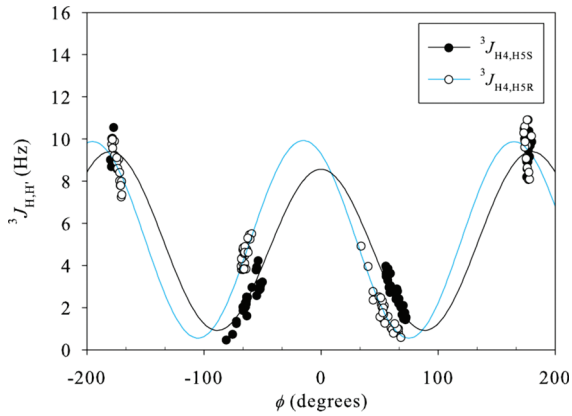

Figure 5. $^3J_{H,H}$ coupling profiles along the C4−C5 bond of methyl α-D-arabinofuranoside. ϕ is the H4−C4−C5−H5(*R*/*S*) dihedral angle.

is maintained (e.g., H2−C2−C3−H3 = 0°), use of a particular equation will give unrealistic values for the corresponding $^3J_{H,H}$ (i.e., $J > 20$ Hz).

$$^3J_{1,2} = 4.62 + 3.16\cos(\phi) + 4.57\cos(2\phi) \quad (5)$$

$$^3J_{2,3} = 8.04 + 8.07\cos(\phi) + 7.24\cos(2\phi) \quad (6)$$

$$^3J_{3,4} = 4.44 + 0.50\cos(\phi) + 4.25\cos(2\phi) \quad (7)$$

The coupling profiles along the C4−C5 bond (Figure 5 and eqs 8 and 9) also illustrate well-fitted ($R^2 = 0.97$) and well-defined Karplus-type relationships. Of particular note, the $^3J_{H4,H5R}$ curve is shifted by ca. 15° from the $^3J_{H4,H5S}$ curve. As a result, a phase factor has been added to eq 9 to obtain a better fit to the DFT data.

$$^3J_{4,5S} = 4.95 - 0.42\cos(\phi) + 4.03\cos(2\phi) \quad (8)$$

$$^3J_{4,5R} = 5.23 + 0.02\cos(\phi + 15.1°) + 4.67\cos(2\phi + 30.2°) \quad (9)$$

The dependence of the $^3J_{H,H}$ values on the rotation of the C5−O5 bond was also investigated. Some variation in the J values as a function of H5−O5−C5−C4 angle was observed, and this analysis is presented in the Supporting Information.

Comparison of DFT/MD-Derived and Experimental $^3J_{H,H}$ Values for 1. With the empirical and DFT-derived relationships (eqs 3 and 5−9, respectively) in hand, and with the use of eq 1, we calculated averaged $^3J_{H,H}$ values using the distribution of conformers we had previously obtained from an MD simulation of **1**.[52] This investigation had identified a single conformer family located in the northeastern portion of the pseudorotational itinerary (Figure 1). Presented in Table 1 is a comparison of these calculated $^3J_{H,H}$ values for **1** with those measured by NMR spectroscopy. Analysis of these data reveals that the DFT-derived eqs 5−9 yield results that are in better agreement with experimental $^3J_{H,H}$ than those calculated using the empirical relationship (eq 3). Indeed, this is observed for all coupling constants, with the exception of $^3J_{H4,H5R}$. The calculated ring couplings ($^3J_{H1,H2}$, $^3J_{H2,H3}$, and $^3J_{H3,H4}$) show the same trend as experiment, with a near perfect agreement observed for $^3J_{H3,H4}$. The calculated $^3J_{H1,H2}$ is slightly larger than the experimental value, which could be attributed to small errors in the conformer distributions obtained from the MD simulations.

Table 1. Comparison of Experimental and Theoretical $\langle^3J_{H,H}\rangle$ Values (in Hz) for **1**[a]

coupling	exp	EK[b]	DK[b]
$\langle^3J_{H1,H2}\rangle$	1.7	2.8	2.4
$\langle^3J_{H2,H3}\rangle$	3.4	5.2	3.8
$\langle^3J_{H3,H4}\rangle$	5.8	8.5	5.8
$\langle^3J_{H4,H5R}\rangle$	5.8	4.2	4.2
$\langle^3J_{H4,H5S}\rangle$	3.3	1.4	3.2

[a] Exp = experimental, EK = empirical Karplus equation, DK = DFT-derived equations. [b] MD simulations led to a conformational distribution largely located in the northeast region of the pseudorotational itinerary (centered around $P \approx 45°$) and a C4−C5 rotamer distribution of approximately 37% gt, 7% tg, and 56% gg.

There is good agreement with the DFT/MD-determined $^3J_{H4,H5S}$ value; however, for $^3J_{H4,H5R}$ significant deviations from experiment are observed. Again, a possible explanation for this discrepancy stems from small differences in the MD-predicted hydroxymethyl rotamer populations and those found in solution. The simulations overestimate the gg rotamer population (56%) compared to experiment (48%) and underestimate the gt rotamer population (37% compared to 45%). In the gt rotamer, H4 and H5R are trans to each other and hence the $^3J_{H,H}$ for this rotamer is large. This coupling is therefore the largest contributor to the average $^3J_{H,H}$, and if the population is underestimated in the MD simulations, then the calculated average coupling would be smaller than the experimental value. Better agreement with the experimental $^3J_{H4,H5R}$ values would be obtained if, in the MD simulation, the population of the gt rotamer is increased and the population of the gg rotamer is decreased. In contrast, the $^3J_{H4,H5S}$ values would remain less affected, as the $^3J_{H4,H5S}$ value is rather insensitive to the relative populations of the gt and gg rotamers (the largest coupling between H4 and H5S is present in the tg rotamer). More information can be found in the Supporting Information. It should be appreciated, however, that differences as low as 0.2 kcal/mol in the relative energies of two rotamers can lead to significantly different rotamer populations. Therefore, differences in energies between MD and solution would need to be less than 0.2 kcal/mol to obtain better agreement.

It is not surprising that the use of the DFT-derived relationships yields better results than the generalized equa-

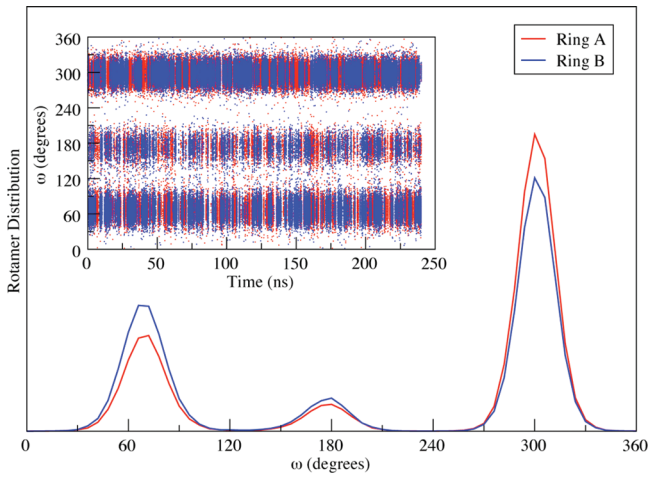

Figure 6. Time dependence of the ω angle (insets) and the resulting histograms obtained from the simulation of **2** for ring A (red) and ring B (blue).

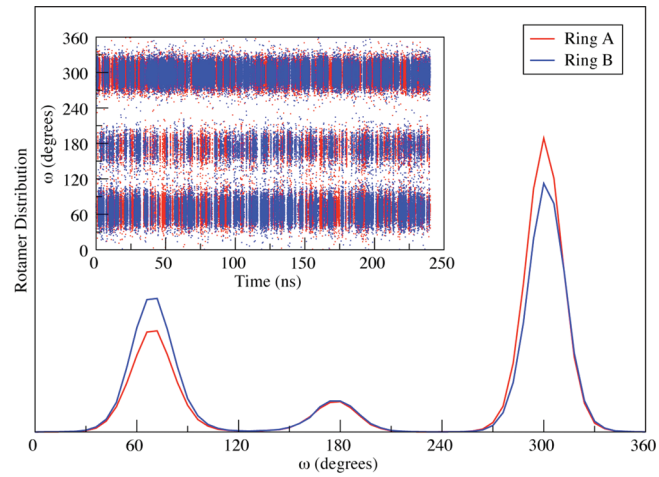

Figure 7. Time dependence of the ω angle (insets) and the resulting histograms obtained from the simulation of **3** for ring A (red) and ring B (blue).

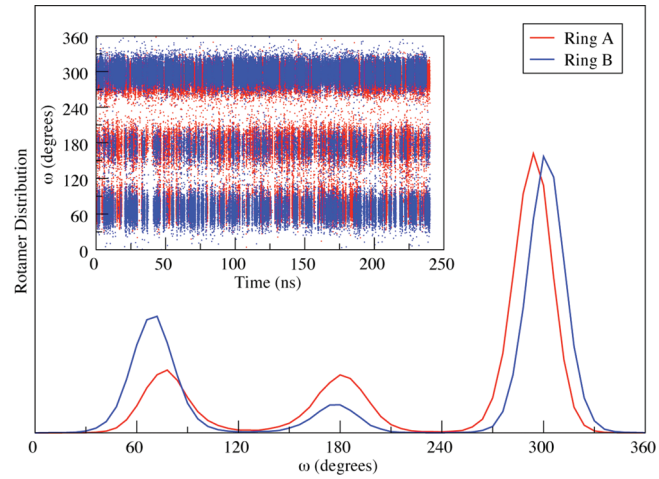

Figure 8. Time dependence of the ω angle (insets) and the resulting histograms obtained from the simulation of **4** for ring A (red) and ring B (blue).

tion. Nevertheless, the difference between the two is striking, with the $^3J_{H,H}$ values differing by an average 1.3 Hz (over a range of 0.4−2.6 Hz). An important implication of this finding is that the results of many previous conformational analyses of α-arabinofuranose rings,[31,83−85] which relied upon the use of generalized relationships such as eq 3, should now be re-evaluated. These previous studies also involved the analysis of $^3J_{H,H}$ by PSEUROT,[47] in which a two-state conformational model is assumed. The results in Table 1 and our previous MD simulations on **1**[52] suggest that the two-state model is not applicable for the α-arabinofuranose ring. Hence, the use of the PSEUROT approach in probing the conformation of these ring systems appears to be of questionable utility. Instead, an alternative approach would be to carry out an AMBER/GLYCAM MD simulation of the α-arabinofuranoside of interest and subsequently use the resulting conformer ensemble to calculate $^3J_{H,H}$ values that can be directly compared with those from experiment (see below). Moreover, use of the dihedral angle distributions from the MD simulations with the DFT-determined equations leads to significantly better agreement than the use of idealized geometrical parameters (e.g., H1−C1−C2−H2 = 180°; see Supporting Information), thus demonstrating that the DFT-determined equations must be used in conjunction with the MD conformer ensemble to reasonably predict the $^3J_{H,H}$ values.

Conformational Analysis of Larger α-Arabinofuranoside Oligomers (2−8). Having had success in applying this approach to monosaccharide **1**, we next turned our attention to larger oligosaccharides containing α-arabinofuranoside residues (**2**−**8**), the conformations of which we have previously investigated.[55] To begin, we carried out MD simulations on disaccharides **2**−**4**, which are the three possible isomeric methyl α-D-arabinofuranosyl-α-D-arabinofuranosides.

Rotamer Populations in 2−4. MD simulations of **2**−**4** required 240 ns for the rotamer populations to achieve convergence to reasonable uncertainties (errors in populations of 3% or less), a simulation time similar to that reported previously for **1**.[52] Figures 6−8 show the time dependence of the ω angle for both rings in each of **2**−**4**, as well as the resulting histograms. Table 2 summarizes the rotamer populations about the C4−C5 bond in each ring for the three disaccharides.

Table 2. MD-Derived Rotamer Populations for Rings A and B of **2**−**4**[a]

	1	**2**		**3**		**4**	
		A	B	A	B	A	B
X_{gt}	37 (3)	25 (2)	34 (2)	27 (2)	35 (2)	17 (2)	30 (2)
X_{tg}	7 (1)	8 (1)	9 (1)	8 (1)	9 (1)	18 (2)	8 (1)
X_{gg}	56 (3)	67 (3)	57 (3)	65 (3)	56 (3)	65 (3)	62 (3)

[a] Standard errors were calculated according to Allen and Tildesley[88] and are reported in parentheses.

The results presented in Figures 6−8 and Table 2 demonstrate that the simulations yield three well-defined rotamers for the C4−C5 bond of each ring in disaccharides **2**−**4**. In the α-(1→2) and α-(1→3)-linked disaccharides, **2** and **3**, respectively, the rotamer populations of both rings exhibit the same trend, namely $X_{gg} > X_{gt} > X_{tg}$, which is in agreement with the results obtained for **1**,[52] as well as experiment.[54,55] However, different results are observed for

Table 3. $^3J_{H4,H5R}$ and $^3J_{H4,H5S}$ (in Hz) for Each Ring in **2**−**4** Obtained from Experiment and from MD Simulation Conformer Populations[a]

		ring A			ring B		
		Exp	EK	DK	Exp	EK	DK
2	*R*	5.8	2.4	3.4	5.8	3.8	4.0
	S	3.1	1.6	3.3	3.3	1.7	3.3
3	*R*	5.8	2.8	3.6	5.8	4.0	4.1
	S	3.4	1.6	3.3	3.4	1.7	3.3
4	*R*	5.5	2.6	3.5	5.5	3.2	3.7
	S	3.4	2.0	3.5	3.4	1.6	3.3

[a] $R = {}^3J_{H4,H5R}$, $S = {}^3J_{H4,H5S}$, Exp = experimental, EK = extended Karplus equation, DK = DFT-derived equation.

the α-(1→5)-linked disaccharide **4**. The rotamer populations of ring B follow the trend observed for the rings in **1**−**3** ($X_{gg} > X_{gt} > X_{tg}$) but those of ring A follow the trend $X_{gg} > X_{tg} \approx X_{gt}$. The results of the simulations in ring A of **4** thus differ from experimental data, which has shown that the C4−C5 bonds in both rings in **4** have similar rotameric distributions.[54] On the basis of these results and those obtained from **1**, it is clear that for "terminal" C4−C5 bonds (all those in **1**−**3** and ring B in **4**) the simulations provide rotamer populations similar to each other and also to experiment. However for "internal" C4−C5 bonds, as for ring A in **4**, poorer agreement with experiment is seen; although the gg rotamer is still the most populated, the tg rotamer is enhanced at the expense of the gt rotamer.

Shown in Table 3 are the $^3J_{H4,H5R}$ and $^3J_{H4,H5S}$ coupling constants measured by NMR spectroscopy,[26,27] as well as those calculated from the conformer ensemble obtained from the simulations by application of the empirical Karplus equation and the DFT-determined equations. These data demonstrate that agreement between the calculated $^3J_{H4,H5R}$ and $^3J_{H4,H5S}$ values and the experimental ones improves significantly by using the DFT-derived equations as opposed to the generalized relationship. In particular, the DFT-derived equation for $^3J_{H4,H5S}$ reproduces the experimental value essentially identically for all three molecules. With regard to $^3J_{H4,H5R}$, the calculated values are all significantly smaller than those obtained from experiment, which is consistent with the monosaccharide **1**, but again better agreement is observed using the DFT-derived equations. Again, this discrepancy may be due to the MD-predicted hydroxymethyl group conformation.

Rotamer Populations in 5−8. We next examined the C4−C5 rotamer populations in four larger oligosaccharides (**5**−**8**, Figure 3); results analogous to those seen in **2**−**4** were observed. Rotamers about C4−C5 bonds involved in an α-(1→5) linkage (rings A and B) exhibit similar dependencies of the ω angle and histograms to that of ring A in disaccharide **4**. In contrast, for terminal C4−C5 bonds (rings C or D), populations similar to those of both rings of disaccharides **2** and **3** and ring B of **4** are obtained (Table 4).

As would be expected from the similarity between the C4−C5 rotamer populations in **5**−**8** with those in **2**−**4**, the trends observed in the $^3J_{H4,H5R}$ and $^3J_{H4,H5S}$ magnitudes are analogous to those described above (Table 5). That is, the use of the DFT-derived equation significantly underestimates

Table 4. MD-Derived Rotamer Populations for the Rings A, B, C, and D of **5**−**8**[a]

		ring A	ring B	ring C	ring D
5	X_{gt}	14 (2)	24 (2)		30 (2)
	X_{tg}	15 (2)	7 (1)		8 (1)
	X_{gg}	71 (3)	69 (3)		62 (3)
6	X_{gt}	14 (2)	13 (2)	32 (2)	
	X_{tg}	16 (2)	15 (2)	8 (1)	
	X_{gg}	70 (3)	72 (3)	60 (3)	
7	X_{gt}		9 (1)	31 (2)	31 (2)
	X_{tg}		22 (2)	9 (1)	8 (1)
	X_{gg}		69 (3)	60 (3)	61 (3)
8	X_{gt}	17 (2)	11 (1)	28 (2)	34 (2)
	X_{tg}	18 (2)	22 (2)	7 (1)	10 (1)
	X_{gg}	65 (3)	67 (3)	65 (3)	56 (3)

[a] Standard errors were calculated according to Allen and Tildesley 86 and are reported in parentheses.

the $^3J_{H4,H5R}$ magnitude while accurately predicting the value for $^3J_{H4,H5S}$. Similar to the results for **2**−**4**, use of the empirical Karplus equation for the coupling pathways in **5**−**8** leads to the correct trend, however, the magnitudes agree very poorly with experiment, and particularly poor agreement is observed for ring B of **7** and **8**, which is glycosylated at both O5 and O3. In both molecules, the calculated C4−C5 rotamer populations are inverted relative to experiment, regardless of whether the DFT-derived or empirically derived curves are used to calculate the $^3J_{H,H}$. Consistent with the results for **1**-**4**, when the DFT-derived relationships (eqs 5−9) are used, the $^3J_{H4,H5S}$ values obtained for the C4−C5 bonds in **5**−**8** agreed well with experiment (in all cases within 0.4 Hz).

Distribution of Ring Conformers. Having investigated the C4−C5 rotamer populations in **1**−**8**, we turned our attention to the ring conformations in the oligomers and the related coupling constants, $^3J_{H1,H2}$, $^3J_{H2,H3}$, and $^3J_{H3,H4}$. Thus, the same analysis carried out for $^3J_{H4,H5R}$ and $^3J_{H4,H5S}$ was performed for the $^3J_{H,H}$ in each furanose residue of oligosaccharides **2**−**8**. As mentioned previously, direct comparison between experimental $^3J_{H,H}$ and those calculated by application of the various coupling relationships to the conformer ensemble obtained from the MD simulation will eliminate errors associated with the two-state model inherent in the PSEUROT[47] approach. Table 6 lists the $^3J_{H1,H2}$, $^3J_{H2,H3}$, and $^3J_{H3,H4}$ determined from NMR spectroscopy,[54] as well as those calculated from the simulations of oligofuranosides **2**−**8**. For the sake of comparison, the data for **1** are included again in Table 6.

Use of either the generalized Karplus equation or the DFT-derived relationships led to the same trend as experiment ($^3J_{H3,H4} > {}^3J_{H2,H3} > {}^3J_{H1,H2}$) in all the compounds. As was demonstrated for **1**, use of the DFT-derived equations lead to $^3J_{H,H}$ magnitudes that agree with experiment better than the use of the empirical relationship,[56] which uniformly overestimates the magnitudes. It should be noted that both equations yield the lowest magnitudes of $^3J_{H1,H2}$, $^3J_{H2,H3}$, and $^3J_{H3,H4}$ for rings substituted at C3, which is also observed experimentally. Taken together, these results suggest that these AMBER/GLYCAM MD simulations provide an accurate distribution of ring conformers and that the discrepancies with the absolute $^3J_{H,H}$ values stem from differences

Table 5. $^3J_{H4,H5R}$ and $^3J_{H4,H5S}$ (in Hz) for Each Ring in **5**−**8** Obtained from Experiment and from MD Simulation Conformer Populations[a]

		ring A			ring B			ring C			ring D		
		Exp	EK	DK	Exp	EK	DK	Exp	EK	DK	Exp	EK	DK
5	*R*	5.4	2.1	3.2	5.8	2.4	3.4				5.9	3.2	3.8
	S	3.1	1.5	3.3	3.2	1.5	3.3				3.1	1.6	3.3
6	*R*	5.9	2.2	3.3	5.7	2.0	3.2	5.8	3.5	3.9			
	S	3.2	1.8	3.4	3.2	1.7	3.3	3.3	1.7	3.3			
7	*R*				5.3	1.9	3.3	5.9	3.4	3.9	6.0	3.3	3.8
	S				3.0	2.4	3.7	3.4	1.7	3.4	3.3	1.6	3.3
8	*R*	5.4	2.5	3.5	5.4	2.2	3.4	5.7	2.9	3.6	5.7	3.9	4.1
	S	3.1	2.1	3.5	3.0	2.4	3.7	3.2	1.6	3.2	3.2	1.8	3.4

[a] $R = {}^3J_{H4,H5R}$, $S = {}^3J_{H4,H5S}$, Exp = experimental, EK = extended Karplus equation, DK = DFT-derived equations.

Table 6. Vicinal Coupling Constants (in Hz) for the Ring Protons for Each Ring in **1**−**8** Obtained from Experiment and from MD Simulation Conformer Populations[a]

		ring A[b]			ring B[b]			ring C[b]			ring D[b]		
		Exp	EK	DK	Exp	EK	DK	Exp	EK	DK	Exp	EK	DK
1	$^3J_{H1,H2}$	1.7	2.8	2.4									
	$^3J_{H2,H3}$	3.4	5.2	3.8									
	$^3J_{H3,H4}$	5.8	8.5	5.8									
2	$^3J_{H1,H2}$	1.6	0.9	1.7	1.6	1.7	2.0						
	$^3J_{H2,H3}$	3.5	3.6	3.0	3.4	4.4	3.5						
	$^3J_{H3,H4}$	6.3	7.5	5.3	6.1	8.2	5.6						
3	$^3J_{H1,H2}$	1.3	0.7	1.8	1.6	1.7	2.0						
	$^3J_{H2,H3}$	2.2	2.9	2.7	3.4	4.4	3.5						
	$^3J_{H3,H4}$	5.5	6.8	4.9	6.2	8.2	5.6						
4	$^3J_{H1,H2}$	1.6	2.4	2.2	1.6	2.5	2.3						
	$^3J_{H2,H3}$	3.1	4.6	3.6	3.1	4.9	3.7						
	$^3J_{H3,H4}$	5.8	8.0	5.5	6.1	8.3	5.7						
5	$^3J_{H1,H2}$	1.7	2.4	2.2	1.2	0.2	1.6				1.6	1.8	2.1
	$^3J_{H2,H3}$	3.4	4.4	3.5	2.2	2.5	2.6				3.4	4.5	3.5
	$^3J_{H3,H4}$	5.4	7.8	5.5	5.8	6.6	4.8				6.2	8.3	5.7
6	$^3J_{H1,H2}$	1.7	2.4	2.3	1.6	2.1	2.2	1.6	2.3	2.2			
	$^3J_{H2,H3}$	3.2	4.5	3.5	3.2	4.3	3.4	3.3	4.8	3.7			
	$^3J_{H3,H4}$	5.9	7.9	5.5	6.0	7.8	5.5	5.9	8.4	5.7			
7	$^3J_{H1,H2}$				1.1	0.5	1.7	1.6	2.0	2.1	1.6	1.8	2.1
	$^3J_{H2,H3}$				2.1	2.8	2.7	3.3	4.6	3.6	3.4	4.5	3.5
	$^3J_{H3,H4}$				5.3	7.0	5.0	5.9	8.4	5.7	6.0	8.3	5.7
8	$^3J_{H1,H2}$	1.8	2.3	2.2	1.2	0.1	1.6	1.6	2.3	2.2	1.6	1.6	2.0
	$^3J_{H2,H3}$	3.4	4.4	3.5	2.0	2.6	2.6	3.3	4.8	3.6	3.3	4.4	3.5
	$^3J_{H3,H4}$	5.9	7.8	5.5	5.5	7.0	5.0	5.8	8.5	5.8	6.0	8.2	5.6

[a] Exp = experimental, EK = extended Karplus equation, DK = DFT-derived equations. [b] See Figure 3 for definition of ring labels.

between the spin−spin coupling profiles derived for **1** and those that could be calculated, for larger, more complicated systems such as **2**−**8**.

We also evaluated the distribution of *P* for all of the rings in these compounds. Similar to what we observed for **1**,[52] unsubstituted rings, or those glycosylated at O2 and O5, display conformational distributions with a single conformer family, located in the northern hemisphere between −60° and 90° (Figure 9, left panel, and Supporting Information). In contrast, for rings substituted at O3 such as ring B of **3**, **5**, **7**, and **8** the distributions of the *P* display a second populated area of conformational space in the southern hemisphere, which is centered about $P = 120°$ (Figure 9, right panel). Thus, attaching another sugar to the ring influences the ring conformation only when this group is attached at O3, not at O2 or O5. This corresponds well to the results obtained by the analysis of $^3J_{H,H}$.

Conclusions

We report here the combined use of AMBER/GLCYAM MD simulations and calculation of $^3J_{H,H}$ ($^3J_{H1,H2}$, $^3J_{H2,H3}$, $^3J_{H3,H4}$, $^3J_{H4,H5R}$, and $^3J_{H4,H5S}$) from the resulting conformer distribution to probe the conformation of a group of oligosaccharides consisting of one to four α-arabinofuranosyl residues (**1**−**8**). This approach allows for the direct comparison of vicinal coupling constants obtained from NMR spectroscopy and conformer populations from MD simulations, thereby circumventing possible sources of errors introduced by the model used to analyze NMR data (e.g., the two-state model inherent in PSEUROT[47] or the "discrete" model[45]).

The coupling constant values calculated from either the DFT-derived $^3J_{H,H}$ relationships or the empirically derived Karplus equation showed, for nearly all cases, the same trend as experiment. These results lend credence to the ability of AMBER/GLYCAM to provide accurate conformer distributions of oligosaccharides containing α-arabinofuranoside rings. Not surprisingly, the DFT-derived equations obtained for **1** lead to significantly better agreement between experiment and theory, compared to the use of an empirical Karplus equation. Indeed, for many of the $^3J_{H,H}$ nearly identical agreement between the calculated values and those obtained from experiment is observed.

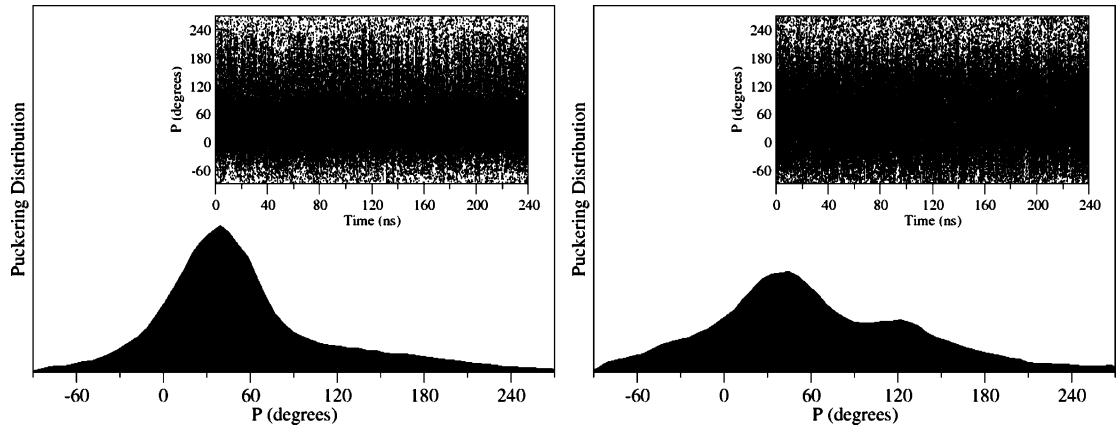

Figure 9. Time dependence of the *P* angle (insets) and the resulting histograms obtained by the simulation of disaccharide **3** ring A (right) and ring B (left).

As determined in earlier studies with monosaccharide **1**,[52] long simulation times (240 ns) are required to achieve convergence. The simulations yield three well-defined rotamers for each ring of the oligofuranosides **2**−**8**. In the particular cases of terminal rotamers, their populations exhibit the trend $X_{gg} > X_{gt} > X_{tg}$. However, internal rotamers, which are defined as those involved in an α-(1→5) linkage, follow a different trend, namely, $X_{gg} > X_{tg} = X_{gt}$; the results for these internal linkages do not agree with experimental data. In the search for the origin of this discrepancy, we evaluated the efficiency of the TIP3P model to represent the water−carbohydrate interactions in **2**−**8** by performing the same simulations using the TIP4P water model (data not shown). The use of this more sophisticated water model led to the same outcome as TIP3P, thus suggesting the difference with experiment is not related to the choice of water model. We postulate that the use of coupling relationships more tailored to these substituted linkages may lead to better agreement between the rotamer populations obtained from the simulations and those determined experimentally.

Another point of poor agreement is the $^3J_{H4,H5R}$ magnitudes in **2**−**8**, for which the calculated values are significantly smaller than those measured by NMR spectroscopy. In attempting to determine the origin of this discrepancy, we considered that it may result from the effect of C5−O5 bond rotation on the magnitude of this $^3J_{H,H}$. However, when this was investigated (see Supporting Information), we found that rotation about this bond has only a minor effect on the coupling across the C4−C5 bond, which is consistent with earlier work by Serianni and co-workers on computed $^3J_{H,H}$ values in hydroxymethyl groups in pyranosides.[39] Currently, investigations are ongoing to elucidate the lack of agreement between the computed and experimental values for $^3J_{H4,H5R}$. A possible alternative approach for the prediction of these couplings would be to sample the MD trajectories for a small set of representative conformers and to perform the DFT coupling calculations directly on these structures. This approach will avoid any possible errors that may be introduced in the fitting of the DFT data to obtain the coupling profiles. Moreover, the possibility that the MD simulations may not accurately predict the C4−C5 rotamer distributions may be a source of the discrepancy in the $^3J_{H4,H5R}$ values. For a more complete determination of the solution conformation of the hydroxymethyl groups in **2**−**8**, measurements of $^2J_{C,H}$, $^3J_{C,H}$, and $^4J_{C,H}$ would provide additional insights. Similar studies have been conducted by Serianni and co-workers, where various coupling constants in ^{13}C-labeled carbohydrates were used to probe conformation.[38−41,86,87] Analogous studies on **1** are currently ongoing.

With regard to ring puckering, the simulations yield *P* distributions for the rings of oligofuranosides **2**−**8** that are essentially identical to those previously determined for the monomer, methyl α-D-arabinofuranoside **1**.[52] The conformers are distributed in the northern hemisphere and thus in a single region of the pseudorotational itinerary. These results confirm our earlier work on **1**, which suggested that the two-state conformational model for assessing ring conformation using PSEUROT is not valid for α-arabinofuranoside rings. On the basis of the simulations carried out here, a notable exception is for rings glycosylated at O3 (for ring B of **3** and **6**−**8**), where a second area of conformational space, centered in the southern hemisphere around $P = 120°$, is populated. The two-state model therefore appears to be valid for these substituted rings.

Acknowledgment. This work was supported by the Alberta Ingenuity Centre for Carbohydrate Science and the Natural Sciences and Engineering Research Council of Canada. We thank Michele Richards for helpful discussions. During the period of this work, D.N.S. held an Izaak Walton Killam Postdoctoral Fellowship. R.E.W. is a Canada Research Chair in Physical Chemistry.

Supporting Information Available: Details on the determination of the spin−spin coupling profiles; analysis of different basis sets and functionals; table of all calculated $^3J_{H,H}$ values; details on the C5−O5 dependence of $^3J_{4,5R}$ and $^3J_{4,5S}$; distributions of H−H dihedral angles, C4−C5 rotamers, and ring pucker obtained from the MD simulations; details of MD/DFT coupling constant calculations; and elaboration on the discrepancies in $^3J_{H4,H5R}$ values. This information is available free of charge via the Internet at http://pubs.acs.org.

References

(1) Dwek, R. A. *Chem. Rev.* **1996**, *96*, 683–720.

(2) Rojo, J.; Morales, J. C.; Penades, S. *Top. Curr. Chem.* **2002**, *218*, 45–92.

(3) Koeller, K. M.; Wong, C. H. *Nat. Biotechnol.* **2000**, *18*, 835–841.

(4) Dwek, R. A.; Butters, T. D. *Chem. Rev.* **2002**, *102*, 283–284.

(5) Meyer, B.; Moller, H. *Top. Curr. Chem.* **2007**, *267*, 187–251.

(6) Wormald, M. R.; Petrescu, A. J.; Pao, Y. L.; Glithero, A.; Dwek, R. A. *Chem. Rev.* **2002**, *102*, 371–386.

(7) Wang, W.; Donini, O.; Reyes, C. M.; Kollman, P. A. *Annu. Rev. Biophys. Biomol. Struct.* **2001**, *30*, 211–243.

(8) Adcock, S. A.; McCammon, J. A. *Chem. Rev.* **2006**, *106*, 1589–1615.

(9) MacKerell, A. D., Jr.; Bashford, D.; Bellott, M.; Dunbrack, R. L., Jr.; Evanseck, J. D.; Field, M. J.; Fischer, S.; Gao, J.; Guo, H.; Ha, S.; Joseph-McCarthy, D.; Kuchnir, L.; Kuczera, K.; Lau, F. T. K.; Mattos, C.; Michnick, S.; Ngo, T.; Nguyen, D. T.; Prodhom, B.; Reiher, W. E., III; Roux, B.; Schlenkrich, M.; Smith, J. C.; Stote, R.; Straub, J.; Watanabe, M.; Wiorkiewicz-Kuczera, J.; Yin, D.; Karplus, M. *J. Phys. Chem. B* **1998**, *102*, 3586–3616.

(10) Oostenbrink, C.; Villa, A.; Mark, A. E.; Van Gunsteren, W. F. *J. Comput. Chem.* **2004**, *25*, 1656–1676.

(11) Jakalian, A.; Bush, B. L.; Jack, D. B.; Bayly, C. I. *J. Comput. Chem.* **2000**, *21*, 132–146.

(12) Jakalian, A.; Bush, B. L.; Jack, D. B.; Bayly, C. I. *J. Comput. Chem.* **2002**, *23*, 1623–1641.

(13) Almond, A.; Petersen, B. O.; Duus, J. *Biochemistry* **2004**, *43*, 5853–5863.

(14) Brisson, J.-R.; Uhrinova, S.; Woods, R. J.; Van der Zwan, M.; Jarrell, H. C.; Paoletti, L. C.; Kasper, D. L.; Jennings, H. J. *Biochemistry* **1997**, *36*, 3278–3292.

(15) Corzana, F.; Motawia, M. S.; Du Penhoat, C. H.; Perez, S.; Tschampel, S. M.; Woods, R. J.; Engelsen, S. B. *J. Comput. Chem.* **2004**, *25*, 573–586.

(16) Gonzalez-Outeirino, J.; Kadirvelraj, R.; Woods, R. J. *Carbohydr. Res.* **2005**, *340*, 1007–1018.

(17) Woods, R. J. *Glycoconjugate J.* **1998**, *15*, 209–216.

(18) Engelsen, S. B.; Cros, S.; Mackie, W.; Perez, S. *Biopolymers* **1996**, *39*, 417–433.

(19) Xia, J.; Daly, R. P.; Chuang, F.; Parker, L.; Jensen, J. H.; Margulis, C. J. *J. Chem. Theory Comput.* **2007**, *3*, 1620–1628.

(20) Xia, J.; Daly, R. P.; Chuang, F.; Parker, L.; Jensen, J. H.; Margulis, C. J. *J. Chem. Theory Comput.* **2007**, *3*, 1629–1643.

(21) Cros, S.; Hervé du Penhoat, C.; Pérez, S.; Imberty, A. *Carbohydr. Res.* **1993**, *248*, 81–93.

(22) French, A. D.; Mouhous-Riou, N.; Pérez, S. *Carbohydr. Res.* **1993**, *247*, 51–62.

(23) Hervé du Penhoat, C.; Engelsen, S. B.; Plusquellec, D.; Pérez, S. *Carbohydr. Res.* **1997**, *305*, 131–145.

(24) Mazeau, K.; Pérez, S. *Carbohydr. Res.* **1998**, *311*, 203–217.

(25) French, A. D.; Kelterer, A.-M.; Cramer, C. J.; Johnson, G. P.; Dowd, M. K. *Carbohydr. Res.* **2000**, *326*, 305–322.

(26) Cros, S.; Imberty, A.; Bouchemal, N.; Hervé du Penhoat, C.; Pérez, S. *Biopolymers* **1994**, *34*, 1433–1447.

(27) Hatcher, E.; Guvench, O.; MacKerell, A. D. *J. Phys. Chem. B* **2009**, 12466–12476.

(28) Brennan, P. J.; Nikaido, H. *Annu. Rev. Biochem.* **1995**, *64*, 29–63.

(29) Li, J.; Lowary, T. L. *Org. Lett.* **2008**, *10*, 881–884.

(30) Altona, C.; Sundaralingam, M. *J. Am. Chem. Soc.* **1972**, *94*, 8205–8212.

(31) Houseknecht, J. B.; Lowary, T. L.; Hadad, C. M. *J. Phys. Chem. A.* **2003**, *107*, 5763–5777.

(32) Kato, K.; Sasakawa, H.; Kamiya, Y.; Utsumi, M.; Nakano, M.; Takahashi, N.; Yamaguchi, Y. *Biochim. Biophys. Acta* **2008**, *1780*, 619–625.

(33) Jimenez-Barbero, J.; Diaz, M. D.; Nieto, P. M. *Anti-Cancer Agents Med. Chem.* **2008**, *8*, 52–63.

(34) Homans, S. W. *Carbohydr. Chem. Biol.* **2000**, *2*, 947–968.

(35) Kraszni, M.; Szakacs, Z.; Noszal, B. *Anal. Bioanal. Chem.* **2004**, *378*, 1449–1463.

(36) Bock, K.; Duus, J. Ø. *J. Carbohydr. Chem.* **1994**, *13*, 513–543.

(37) Bose-Basu, B.; Klepach, T.; Bondo, G.; Bondo, P. B.; Zhang, W.; Carmichael, I.; Serianni, A. S. *J. Org. Chem.* **2007**, *72*, 7511–7522.

(38) Olsson, U.; Serianni, A. S.; Stenutz, R. *J. Phys. Chem. B* **2008**, *112*, 4447–4453.

(39) Pan, Q.; Klepach, T.; Carmichael, I.; Reed, M.; Serianni, A. S. *J. Org. Chem.* **2005**, *70*, 7542–7549.

(40) Klepach, T. E.; Carmichael, I.; Serianni, A. S. *J. Am. Chem. Soc.* **2005**, *127*, 9781–9793.

(41) Thibaudeau, C.; Stenutz, R.; Hertz, B.; Klepach, T.; Zhao, S.; Wu, Q.; Carmichael, I.; Serianni, A. S. *J. Am. Chem. Soc.* **2004**, *126*, 15668–15685.

(42) Minch, M. J. *Concepts Magn. Reson.* **1994**, *6*, 41–56.

(43) Contreras, R. H.; Peralta, J. E. *Prog. Nucl. Magn. Reson. Spectrosc.* **2000**, *37*, 321–425.

(44) Coxon, B. *Adv. Carbohydr. Chem. Biochem.* **2009**, *62*, 17–82.

(45) Dzakula, Z.; Westler, W. M.; Edison, A. S.; Markley, J. L. *J. Am. Chem. Soc.* **1992**, *114*, 6195–6199.

(46) Dzakula, Z.; DeRider, M. L.; Markley, J. L. *J. Am. Chem. Soc.* **1996**, *118*, 12796–12803.

(47) Deleeuw, F.; Altona, C. *J. Comput. Chem.* **1983**, *4*, 428–437.

(48) Gonzalez-Outeirino, J.; Kirschner, K. N.; Thobhani, S.; Woods, R. J. *Can. J. Chem.* **2006**, *84*, 569–579.

(49) Kirschner, K. N.; Woods, R. J. *Proc. Natl. Acad. U.S.A.* **2001**, *98*, 10541–10545.

(50) Basma, M. D.; Calgan, Varnali, T.; Woods, R. J. *J. Comput. Chem.* **2001**, *22*, 1125–1137.

(51) Woods, R. J.; Chappelle, R. *J. Mol. Struct.* **2000**, *527*, 149–156.

(52) Seo, M.; Castillo, N.; Ganzynkowicz, R.; Daniels, C.; Woods, R.; Lowary, T. L.; Roy, P.-N. *J. Chem. Theory Comput.* **2008**, *4*, 184–191.

(53) Taha, H. A.; Castillo, N.; Roy, P.-N.; Lowary, T. L. *J. Chem. Theory Comput.* **2009**, *5*, 430–438.

(54) D'Souza, F. W.; Ayers, J. D.; McCarren, P. R.; Lowary, T. L. *J. Am. Chem. Soc.* **2000**, *122*, 1251–1260.

(55) Houseknecht, J. B.; Altona, C.; Hadad, C. M.; Lowary, T. L. *J. Org. Chem.* **2002**, *67*, 4647–4651.

(56) Altona, C.; Francke, R.; de Haan, R.; Ippel, J. H.; Daalmans, G. J.; Hoekzema, A. J. A. W.; van Wijk, J. *Magn. Reson. Chem.* **1994**, *32*, 670–678.

(57) Sauer, S. *Int. J. Mol. Sci.* **2003**, *4*, 62–63.

(58) Alkorta, I.; Elguero, J. *Int. J. Mol. Sci.* **2003**, *4*, 64–92.

(59) Zaccari, D.; Barone, V.; Peralta, J. E.; Contreras, R. H.; Taurian, O. E.; Díez, E.; Esteban, A. *Int. J. Mol. Sci.* **2003**, *4*, 93–106.

(60) Zubkov, S. V.; Chertkov, V. A. *Int. J. Mol. Sci.* **2003**, *4*, 107–118.

(61) Ruud, K.; Frediani, L.; Cammi, R.; Mennucci, B. *Int. J. Mol. Sci.* **2003**, *4*, 119–134.

(62) Jackowski, K. *Int. J. Mol. Sci.* **2003**, *4*, 135–142.

(63) Pecul, M.; Helgaker, T. *Int. J. Mol. Sci.* **2003**, *4*, 143–157.

(64) Autschbach, J.; Le Guennic, B. *J. Chem. Educ.* **2007**, *84*, 156–171.

(65) Vaara, J.; Jokisaari, J.; Wasylishen, R. E.; Bryce, D. L. *Prog. Nucl. Magn. Reson. Spectrosc.* **2002**, *41*, 233–304.

(66) Vahtras, O.; Ågren, H.; Jørgensen, P.; Jensen, H. J. A.; Padkjaer, S. B.; Helgaker, T. *J. Chem. Phys.* **1992**, *99*, 6120–6125.

(67) Helgaker, T.; Jaszuñski, M.; Pecul, M. *Prog. Nucl. Magn. Reson. Spectrosc.* **2008**, *53*, 249–268.

(68) Frisch, M. J.; Trucks, G. W.; Schlegel, H. B.; Scuseria, G. E.; Robb, M. A.; Cheeseman, J. R.; Montgomery, J. A., Jr.; Vreven, T.; Kudin, K. N.; Burant, J. C.; Millam, J. M.; Iyengar, S. S.; Tomasi, J.; Barone, V.; Mennucci, B.; Cossi, M.; Scalmani, G.; Rega, N.; Petersson, G. A.; Nakatsuji, H.; Hada, M.; Ehara, M.; Toyota, K.; Fukuda, R.; Hasegawa, J.; Ishida, M.; Nakajima, T.; Honda, Y.; Kitao, O.; Nakai, H.; Klene, M.; Li, X.; Knox, J. E.; Hratchian, H. P.; Cross, J. B.; Bakken, V.; Adamo, C.; Jaramillo, J.; Gomperts, R.; Stratmann, R. E.; Yazyev, O.; Austin, A. J.; Cammi, R.; Pomelli, C.; Ochterski, J. W.; Ayala, P. Y.; Morokuma, K.; Voth, G. A.; Salvador, P.; Dannenberg, J. J.; Zakrzewski, V. G.; Dapprich, S.; Daniels, A. D.; Strain, M. C.; Farkas, O.; Malick, D. K.; Rabuck, A. D.; Raghavachari, K.; Foresman, J. B.; Ortiz, J. V.; Cui, Q.; Baboul, A. G.; Clifford, S.; Cioslowski, J.; Stefanov, B. B.; Liu, G.; Liashenko, A.; Piskorz, P.; Komaromi, I.; Martin, R. L.; Fox, D. J.; Keith, T.; Al-Laham, M. A.; Peng, C. Y.; Nanayakkara, A.; Challacombe, M.; Gill, P. M. W.; Johnson, B.; Chen, W.; Wong, M. W.; Gonzalez, C.; and Pople, J. A. *Gaussian 03, Revision E.01*; Gaussian, Inc.: Wallingford, CT, 2004.

(69) Helgaker, T.; Watson, M.; Handy, N. C. *J. Chem. Phys.* **2000**, *113*, 9402–9409.

(70) Becke, A. D. *J. Chem. Phys.* **1993**, *98*, 5648–5652.

(71) Marquardt, D. *SIAM J. Appl. Math.* **1963**, *11*, 431–441.

(72) Haasnoot, C. A. G.; De Leeuw, F. A. A. M.; Altona, C. *Tetrahedron* **1980**, *36*, 2783–2792.

(73) Case, D. A.; Darden, T. A.; Cheatham, T. E., III; Simmerling, C. L.; Wang, J.; Duke, R. E.; Luo, R.; Merz, K. M.; Pearlman, D. A.; Crowley, M.; Walker, R. C.; Zhang, W.; Wang, B.; Hayik, S.; Roitberg, G.; Seabra, G.; Wong, K. F.; Paesani, F.; Wu, X.; Brozell, S.; Tsui, V.; Gohlke, H.; Yang, L.; Tan, C.; Mongan, J.; Hornak, V.; Cui, G.; Beroza, P.; Mathews, D. H.; Schafmeister, C.; Ross, W. S.; Kollman, P. A. *AMBER 9*; University of California, San Francisco, 2006.

(74) Woods, R. J.; Dwek, R. A.; Edge, C. J.; Fraser-Reid, B. *J. Phys. Chem.* **1995**, *99*, 3832–3846.

(75) Case, D. A.; Cheatham, T. E.; Darden, T.; Gohlke, H.; Luo, R.; Merz, K. M.; Onufriev, A.; Simmerling, C.; Wang, B.; Woods, R. J. *J. Comput. Chem.* **2005**, *26*, 1668–1688.

(76) Cieplak, P.; Cornell, W. D.; Bayly, C.; Kollman, P. A. *J. Comput. Chem.* **1995**, *16*, 1357–1377.

(77) Cornell, W. D.; Cieplak, P.; Bayly, C.; Gould, I. R.; Merz, K. M., Jr.; Fergunson, D. M.; Spellmeyer, D. C.; Fox, T.; Caldwell, J. W.; Kollman, P. A. *J. Am. Chem. Soc.* **1995**, *117*, 5179–5197.

(78) Berendsen, H. J. C.; Postma, J. P. M.; van Gunsteren, W. F.; DiNola, A.; Haak, J. R. *J. Chem. Phys.* **1984**, *81*, 3684–3690.

(79) Jorgensen, W. L.; Chandrasekhar, J.; Madura, J. D.; Impey, R. W.; Klein, M. L. *J. Chem. Phys.* **1983**, *79*, 926–935.

(80) Ryckaert, J. P.; Ciccotti, G.; Berendsen, H. J. C. *J. Comput. Phys.* **1977**, *23*, 327–341.

(81) Darden, T.; York, D.; Pedersen, L. *J. Chem. Phys.* **1993**, *98*, 10089–10092.

(82) Essmann, U.; Perera, L.; Berkowitz, M. L.; Darden, T.; Lee, H.; Pedersen, L. G. *J. Chem. Phys.* **1995**, *103*, 8577–8593.

(83) Houseknecht, J. B.; McCarren, P. R.; Lowary, T. L.; Hadad, C. M. *J. Am. Chem. Soc.* **2001**, *123*, 8811–8824.

(84) Houseknecht, J. B.; Lowary, T. L.; Hadad, C. M. *J. Phys. Chem. A.* **2003**, *107*, 372–378.

(85) Hoffmann, R. A.; Van Wijk, J.; Leeflang, B. R.; Kamerling, J. P.; Altona, C.; Vliegenthart, J. F. G. *J. Am. Chem. Soc.* **1992**, *114*, 3710–3714.

(86) Zhao, H.; Pan, Q.; Zhang, W.; Carmichael, I.; Serianni, A. S. *J. Org. Chem.* **2007**, *72*, 7071–82.

(87) Klepach, T.; Zhang, W.; Carmichael, I.; Serianni, A. S. *J. Org. Chem.* **2008**, *73*, 4376–4387.

(88) Allen, M. P.; Tildesley, D. J. *Computer Simulation of Liquids*; Oxford University Press Inc.: New York, 1987; pp 192.

CT900477X